Optical Imaging and Magnetic Field Targeting of Magnetic Nanoparticles in Tumors

Susan P. Foy,[†] Rachel L. Manthe,[†] Steven T. Foy,[†] Sanja Dimitrijevic,[†] Nishanth Krishnamurthy,[†] and Vinod Labhasetwar[†,‡,*]

[†]Department of Biomedical Engineering, Lerner Research Institute and [‡]Taussig Cancer Institute, Cleveland Clinic, Cleveland, Ohio 44195

ABSTRACT To address efficacy issues of cancer diagnosis and chemotherapy, we have developed a magnetic nanoparticle (MNP) formulation with combined drug delivery and imaging properties that can potentially be used in image-guided drug therapy. Our MNP consists of an iron-oxide magnetic core coated with oleic acid (OA) and stabilized with an amphiphilic block copolymer. Previously, we reported that our MNP formulation can provide prolonged contrast for tumor magnetic resonance imaging and can be loaded with hydrophobic anticancer agents for sustained drug delivery. In this study, we developed MNPs with optical imaging properties using new near-infrared dyes to quantitatively determine their long-term biodistribution and tumor localization with and without an external magnetic field in mice with xenograft breast tumors. MNPs localized slowly in the tumor, reaching a peak 48 h post-injection before slowly declining over the next 11 days. One hour exposure of the tumor to a magnetic field further enhanced MNP localization to tumors. Our MNPs can be developed with combined drug delivery and multimodal imaging properties to improve cancer diagnosis, provide sustained treatment, and monitor therapeutic effects in tumors over time.

KEYWORDS: tumor targeting · biodistribution · drug delivery systems · fluorophores · theranostic agent

Nanoparticles are a promising theranostic agent with applications for tumor imaging and targeted cancer drug delivery. New designs in nanoparticle formulations take advantage of synergism of multiple imaging modalities to improve cancer diagnosis and treatment and to monitor response to therapy.[1] Two such complementary techniques are magnetic resonance imaging (MRI) and optical imaging. Magnetic resonance imaging provides excellent deep tissue contrast and spatial resolution; however, it is not a quantitative technique, and it is quite costly.[2] Optical imaging is inexpensive, sensitive, and provides excellent spatial and temporal resolution, but penetration is limited to a few millimeters below the tissue.[3] By designing nanoparticle formulations with dual imaging applications, the advantages of MRI as a diagnostic tool can be combined with optical imaging to quantitatively track and determine the biodistribution of nanoparticles *in vivo*.

Formulations of magnetic nanoparticles (MNPs) that combine MRI and optical imaging encapsulate iron-oxide and fluorophores in emulsions or polymeric nanocapsules[4−6] or conjugate fluorophores to the surface of the nanoparticles.[7−9] These techniques produce constructs that can be successfully imaged with MRI and optical imaging; however, some investigators report challenges with these techniques. Iron-oxide blocks the fluorescent signal in encapsulated formulations,[5,9] and chemical conjugates, particularly amide bonds, are susceptible to cleavage *in vivo*.[10] Chemical conjugation can be technically challenging and may alter the charge and biodistribution profile of nanoparticles.[10,11] Multiple agents may compete for the same surface binding sites, altering the efficacy of one or both agents.[12] In addition, the surface-conjugated dye may be cleaved quickly, hindering the long-term *in vivo* biodistribution study of MNPs. Thus, it is beneficial when designing a particle for multifunctional applications to encapsulate agents and limit the number of targeting, therapeutic, and imaging ligands conjugated to the surface.

Our laboratory has developed a unique multifunctional magnetic nanoparticle formulation that consists of an iron-oxide core surrounded by a hydrophobic oleic acid (OA) layer and coated with a Pluronic block copolymer.[13] Pluronic coating anchors to the OA and provides aqueous dispersion for the MNPs, prolonging the circulation time of the MNPs *in vivo* visible with MRI.[14,15] A major advantage of our MNP design is that hydrophobic agents, such as anticancer agents or fluorophores, partition into the OA layer of the particle alone or in combination (Figure 1A).[13,14] This method minimizes

*Address correspondence to labhasv@ccf.org.

Received for review June 24, 2010 and accepted August 17, 2010.

Published online August 23, 2010.
10.1021/nn101427t

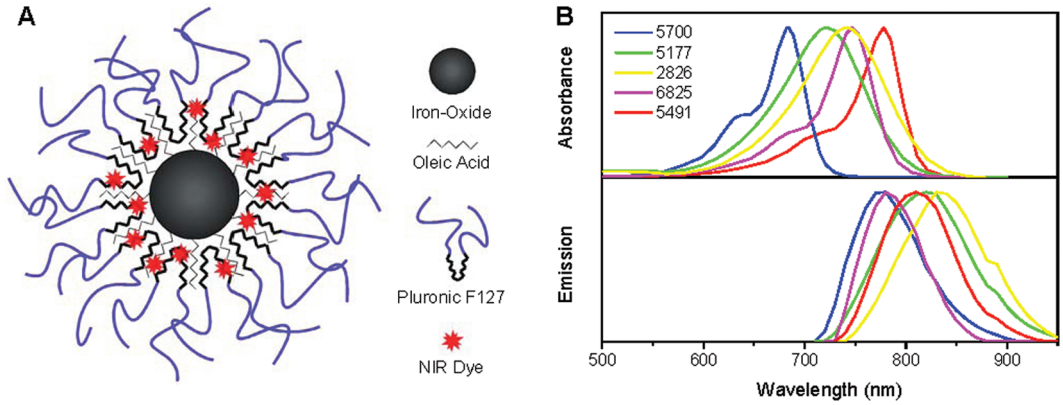

Figure 1. (A) Schematic of a magnetic nanoparticle with fluorescent dye loaded in the hydrophobic oleic acid layer. (B) Absorbance and emission spectra of five NIR dyes tested for optical imaging in MNPs.

changes to the surface characteristics and eliminates the multistep conjugation techniques usually needed to achieve optical imaging and therapeutic properties within the same particle.

The ultimate goal of our MNP design is to increase the delivery of MNPs, and therefore drug, to tumors, as well as aid in diagnosis and evaluation of tumor response with complementary imaging techniques. Incorporating fluorophores within our MNP formulation will also allow us to determine how changes in the formulation and targeting mechanisms alter the biodistribution and accumulation of the MNPs in the tumor over time. The goals of the present study are to (a) select near-infrared (NIR) hydrophobic dyes with strong fluorescence intensity and low toxicity that can be loaded into our MNPs for optical imaging, (b) determine the *in vivo* biodistribution of MNPs in tumor-bearing mice by optical imaging, and (c) optically compare the passive accumulation of MNPs within the tumor to MNPs actively targeted to the tumor by an externally applied magnetic field (MF).

Nanoparticles offer great potential for cancer diagnosis and preoperative planning with MRI,[16] as an intraoperative technique to optically define tumor margins,[16,17] and in targeted drug therapy to achieve chemotherapeutic tumor regression.[18] In addition, dyes that are fluorescent in the NIR region can penetrate ~10 cm through tissue, an ideal penetration depth for breast cancer imaging.[19] We believe this study is significant because our results show that multifunctional and multimodal capabilities within a single novel nanoparticle formulation have a number of potential applications in MRI and drug delivery. With the addition of spectrally distinct fluorophores and active targeting, our MNP formulation offers great promise for the evaluation of different nanoparticle formulations and the advancement of cancer diagnosis and treatment.

RESULTS AND DISCUSSION

In this study, we tested multiple dyes in the NIR window to optimize our MNP formulation for biodistribution analysis. We used a mouse xenograft breast tumor model to test passive MNP accumulation *versus* active targeting with a MF.

To determine whether our MNPs could be used for optical imaging, we tested five commercially available NIR dyes in our MNP formulation and compared their stability, toxicity, and level of fluorescence. These dyes have not been tested for optical imaging for biomedical applications but have been used for applications in credit and security card technology and as inks for laser reading devices. However, the characteristics of the dyes, particularly their hydrophobic nature and NIR excitation and emission wavelengths, are considered suitable for incorporation in our MNPs for *in vivo* imaging. The absorbance curves for each dye when dissolved in ethanol and the emission spectra are shown in Figure 1B. Peak absorbance ranged from 683 to 775 nm (dyes 5700 and 5491) and peak emission ranged from 773 to 830 nm (dyes 5700 and 2826).

The hydrophobic dyes were each dissolved in ethanol and added to the MNPs with overnight stirring at concentrations between 0.25 and 5.0% w/w MNPs. The dyes partitioned into the OA layer of the MNP formulation with 100% loading efficiency for dyes 5700, 5177, 2826, and 5491 at all concentrations tested. Dye 6825 loaded into the MNPs at 100% for the lowest four concentrations (0.25−2.0% w/w); however, at 5% w/w, dye 6825 did not partition into the MNPs because the MNPs had aggregated on the stir bar and could not be recovered. We have used this simple method to load hydrophobic anticancer agents for doxorubicin (base) and/or paclitaxel within the OA layer of our MNPs with high loading efficiency and sustained release over several weeks.[13,14] Although the dye is not chemically conjugated to our MNPs, strong hydrophobic interactions with the OA layer of the MNPs trap the dye within the particles, preventing its rapid leaching (Figure 1).

The size and charge of the particles did not change with the addition of the NIR dyes at the concentrations tested. The size of the iron-oxide core, as determined by transmission electron microscopy, was approximately

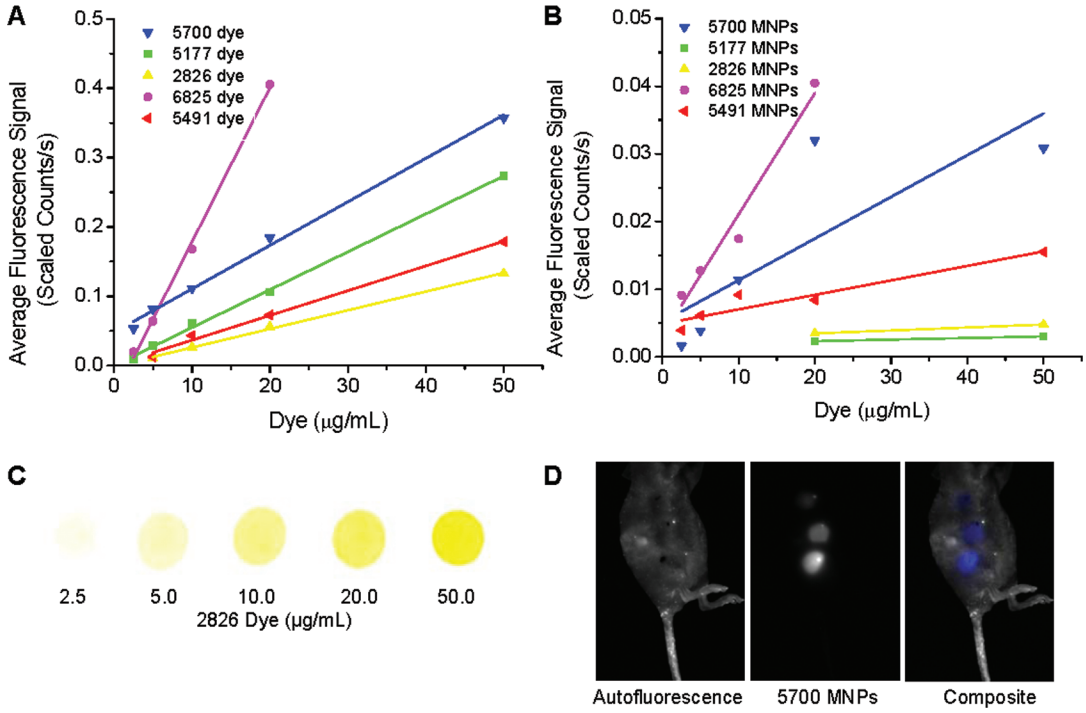

Figure 2. Fluorescence of NIR dyes *in vitro* (A) and dye-loaded MNPs *in vivo* (B). A small amount (3 μL) of each hydrophobic dye in ethanol was dropped onto filter paper and the fluorescence intensity measured with manually drawn regions of interest. Magnetic nanoparticles containing 0.25−5.0% w/w dye were suspended in mannitol citrate buffer (1 mg MNPs/mL), and 20 μL was subcutaneously injected and immediately imaged. Representative images are shown for dye 2826 in ethanol (C), and a mouse subcutaneously injected with MNPs loaded with dye 5700 at 0.25, 0.5, and 1.0% w/w dye in 1 mg/mL MNPs (D).

10−25 nm,[14] with a hydrodynamic diameter of ~240 nm, as determined by dynamic light scattering. The zeta potential of plain and dye-loaded MNPs was about −30 mV. By avoiding chemically conjugating the dye to the surface, the surface properties were not altered by the charge of the dye, an important feature because the surface charge can alter the biodistribution profile of nanoparticles.[10]

For *in vivo* experiments, mice were anesthetized and continuously exposed to NIR light over 20 min to determine if photobleaching would be an issue while imaging over several days. We selected this time frame because each daily image would result in NIR light exposure for less than 2 min over several days for biodistribution studies. We saw a <1% change in signal intensity over the body of the mouse over the 20 min of imaging. Because body tissues scatter and absorb the light, the tissue appears to act as a protective barrier, actually limiting photobleaching of the dyes *in vivo*. We concluded that images taken daily to track the long-term biodistribution of MNPs would be accurate and quantifiable, and we would not need to correct for photobleaching. To evaluate the potential toxicity of the dyes, the IC_{50} for each of the dye−MNP formulations was determined *in vitro* in an MCF7 cell line. At the concentrations tested, MNPs did not inhibit cell growth, whereas MNPs loaded with dye 5700 were the most toxic with the lowest IC_{50}, followed by MNPs loaded with dyes 2826, 6825, 5491, and 5177.

We imaged each dye *in vitro* and dye−MNPs *in vivo* at varying concentrations to evaluate which dyes were more intensely fluorescent (Figure 2). The baseline intensity of dye 5700 was much higher than that of the other dyes tested. Small increases in the concentrations of dye 6825 provided the greatest increase in the fluorescence signal detected (Figure 2A,C). The *in vivo* fluorescence signal intensity of dye−MNPs injected subcutaneously generally paralleled the trends of the *in vitro* fluorescence signal, with a decrease in the signal intensity due to scattering and absorbance of the fluorescence within the tissues (Figure 2B,D).

On the basis of the toxicity and *in vivo* fluorescence intensity studies, we concluded that dyes 5700, 6825, and 5491 were more suitable than dyes 2826 and 5177 for tracking the *in vivo* biodistribution of the MNPs. We did not observe any toxic side effects in the animals injected with dye-loaded MNPs. These observations, in combination with previous studies evaluating the biocompatibility of MNPs in rats,[20] suggest that both plain and dye-loaded MNPs do not cause deleterious effects in rats or mice at the MNP concentrations tested.

An important application relative to our design is the ability to visualize multiple fluorescent species simultaneously, as the dyes are spectrally distinct. Dyes 6825 and 5700 can be easily unmixed from dye 5491, but their spectra overlap enough such that they cannot be unmixed from each other. Because the different fluorophores can easily be loaded into MNPs, conjugating

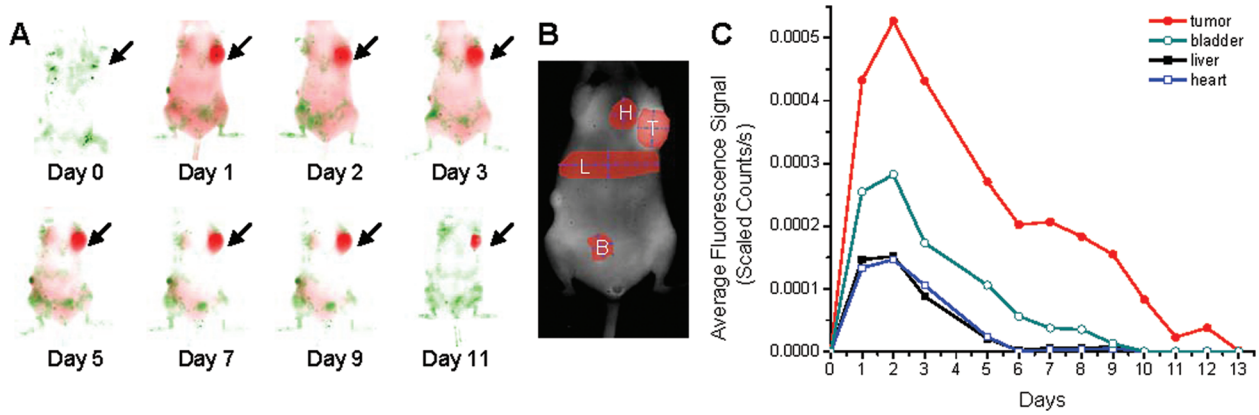

Figure 3. Distribution of Pluronic F127-coated MNPs loaded with the NIR dye 5491 in an athymic nude mouse with a xenograft breast tumor. A mouse was injected with a 100 μL suspension of MNPs in mannitol citrate buffer (4.9 mg MNPs/mL, 5.0% w/w dye) and imaged each day with the Maestro EX imaging system using the blue and NIR excitation and emission filter sets (A). Autofluorescence is shown in green, MNPs loaded with dye 5491 in red. Arrow denotes tumor. Signal intensity of these MNPs in the tumor (T), bladder (B), liver (L), and heart (H) was determined from ROIs drawn over the area of each organ (B,C). Biodistribution was tested in multiple tumor-bearing mice with varying dyes and dye concentrations. The same general trends of high signal intensity measured in the tumor were observed. Figure is representative data with one of the dyes loaded in MNPs.

the particles to different receptors could aid in tumor identification *in vivo* and in distinguishing between subsequent doses of nanoparticles loaded with dye and therapeutic agents.

We next evaluated the *in vivo* biodistribution of our MNPs in a mouse model with xenograft breast tumors. MNPs containing dye 5491 (5.0% w/w) were intravenously injected *via* tail vein and imaged daily with the Maestro Blue and NIR filter sets. One day after injection, the dye−MNPs were easily visible in the subcutaneous MCF7 breast tumor (Figure 3A). Regions of interest (ROIs) drawn over the tumor, bladder, liver, and heart were used to quantify the change in signal intensity each day until no signal was seen (Figure 3B,C). The dye−MNPs in the tumor are more easily quantified because the tumor is subcutaneous. Regions over the bladder, liver, and heart provide a baseline for background fluorescence but are not accurate representations of the amount of MNPs present in these organs because a great deal of the signal is lost due to scatter and absorbance within the tissue for these deeper organs. Fluorescence molecular tomography, or 3-D imaging machines, may provide more accurate biodistribution of MNPs to other body compartments.

The distribution of dye−MNPs follows a traditional one-compartment pharmacokinetic model with prolonged absorption and an increase in signal intensity over the first 2 days, followed by elimination of the particles and dye from the tumor region over 11 days. Generally, the tumor signal to background fluorescence ratio was low during the first 24 h but increased dramatically after strong signal clearance by the liver and intestines. The hydrophobic dyes were dissolved in ethanol and loaded into our MNP formulation for *in vivo* applications. These dyes partition into OA around the iron-oxide core (Figure 1A). We could not find a suitable nontoxic medium to dissolve dyes to observe their biodistribution without MNPs. Nanoparticles are known to localize in tumors due to the enhanced permeability and retention effect because of leaky tumor vasculature and impaired lymphatic drainage.[21] Hence, the biodistribution and clearance kinetics of free dye and dye encapsulated in MNPs is expected to be different.

Interactions of nanoparticles with the components of the reticulo-endothelial system (RES)[22] and other factors, such as size, shape, surface properties (charge, hydrophilicity/hydrophobicity, *etc.*),[23] targeting ligands, and vascular porosity, can influence the tumor targeting efficiency of nanoparticles.[24] The *in vivo* stability of nanoparticles is important to achieve prolonged systemic circulation and tumor targeting of nanoparticles. Therefore, significant effort is now focused on understanding how nanoparticles behave *in vivo*.[25]

The ability of our MNPs to remain in the circulation and extravasate into the tumor mass could be due to the combined effect of its hydrophilic and flexible structure. This could have prevented the MNPs opsonization and clearance by circulating monocytes. To support the above view, we did not see any change in particle size of our MNPs in the presence of protein.[15] Our MNP structure is mostly flexible, except the magnetic core, which is only ~12 nm in diameter. In general, flexible structures provide better systemic circulation than rigid nanostructures of the same diameter. More than the size, perhaps it is the nanoparticle structure and its stability *in vivo* that has the greater influence on the systemic clearance of nanoparticles. For example, ultrasmall (8.7 nm) citrate-coated superparamagnetic iron-oxide nanoparticles have the shortest half-life because of their highly anionic surface charge.[26] Feridex IV mainly localizes in the liver, despite its small size (hydrodynamic mean diameter = 143 nm), because the dextran coating equilibrates with

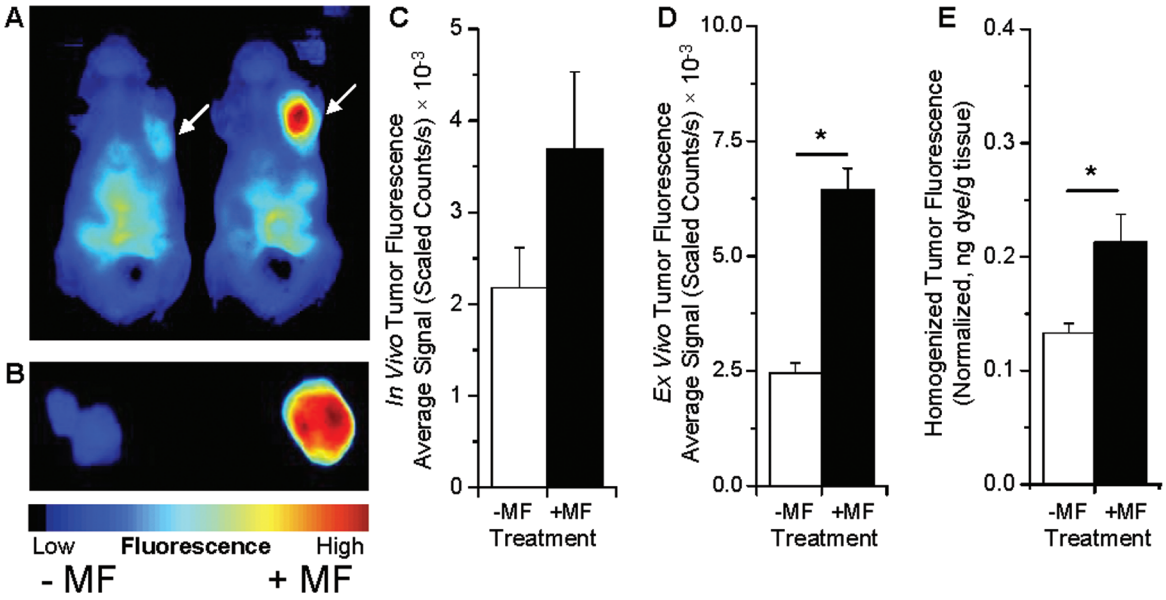

Figure 4. Tumor localization of NIR dye−MNPs increases with 1 h MF treatment. Mice bearing MCF7 xenograft breast tumors were injected with 0.25% w/w MNPs loaded with dye 6825 and subjected (+MF) or not subjected (−MF) to the MF for 1 h. At 24 h post-injection, mice were imaged *in vivo* (A); arrows point to tumors. Animals were euthanized and perfused with saline, and the tumors were extracted and imaged (B). Blue indicates low fluorescence, red high fluorescence in panels A and B. The fluorescence signal was measured from an ROI drawn around the whole tumors *in vivo* (C), *ex vivo* (D), and from the homogenized tumors in a 96-well plate (E). Homogenate was normalized based on the position of the tumor in a 96-well plate. All fluorescence images were acquired with the Maestro EX *in vivo* imaging system with the NIR filter set. Data are shown as mean ± SEM ($n = 4-5$), $*p = 0.05$.

the surrounding medium,[27] and hence it dissociates from the magnetic core, causing particles to aggregate following its intravenous injection.

To determine if we could use optical imaging as an *in vivo* technique to evaluate how targeting might affect the tumor accumulation of MNPs, we compared the passive accumulation of MNPs with MNPs actively targeted to the tumor by an externally applied MF. Mice were anesthetized and intravenously injected with MNPs and then either did (+MF) or did not (−MF) undergo a 1 h MF treatment. At 24 h post-injection, the mice were imaged for accumulation of MNPs (Figure 4). Images of tumors *in vivo* (Figure 4A,C), tumors *ex vivo* isolated following perfusion of animals (Figure 4B,D), and fluorescence from the tumor homogenate (Figure 4E) were on average greater in each of the mice exposed to the MF. We examined the tumors *ex vivo* and the fluorescence from the homogenate to confirm that the signal originated from within the tumor and because of concern that scatter and absorbance from the surrounding tissue might not provide an accurate representation of the signal present. This scatter and absorbance likely explains why the tumor fluorescence varies from *in vivo* to *ex vivo* (panel C *vs* D in Figure 4). We also see a slight difference in the fold increase in tumor fluorescence with and without MF based on *ex vivo* imaging and the tumor homogenate (panel D *vs* E in Figure 4). This may be because we detect fluorescence in the periphery of the tumor while imaging the whole organ *ex vivo*. Additionally, MNPs may not localize to the necrotic tumor core, and the MF provides greater strength to the periphery of the tumor. Despite these differences in the fluorescence measurements, it is clearly evident that the MF results in greater tumor localization of MNPs. The signal intensity in the tumor as a percent of the total from all other organs (heart, lungs, liver, spleen, kidneys, and brain) was 1.5% (−MF) and 3.5% (+MF) from ROIs drawn *ex vivo* over the whole organs. Since the animals were perfused with saline prior to isolating tumors for *ex vivo* imaging, the fluorescence seen is most likely due to MNPs localized in the tumor interstial space and cells rather than in tumor vasculature. It would be interesting to confirm the spatial distribution of dye−MNPs in the tumor histologically; however, a dye with a lower wavelength would be necessary to visualize the fluorescence by confocal microscopy.

We have shown that a short (1 h) exposure to a MF can produce a detectable difference of particles 24 h later verified with optical imaging. However, other investigators have used constant external MF exposure of 2 h, 8 h, or 10 days, then immediately euthanized the animals after removing the MF because of concerns that removing the magnet might result in reversible accumulation of magnetic particles or magnetically labeled cells.[28−30] Our study demonstrates that, even if the MF is removed, the shorter exposure time was sufficient to significantly increase the accumulation evidenced by strong fluorescence signal intensity 24 h post-injection. Since animals were perfused before

collecting the tumor, the signal seen is due to the MNPs localized into tumor tissue and not MNPs within the tumor blood vessels.

Phase 1 clinical trials with magnetically targeted drug particles were clinically effective in reducing tumor growth, and particles were detected through histological methods up to 6 weeks post-injection with only 1 to 2 h MF exposure.[31] This clinical trial suggests that, although a significant fraction of particles are cleared by the liver and the RES during the first 48 h, the larger size of the particles, as well as firm and constant MF exposure, may be key to attracting MNPs over a long distance and to retaining particles even under conditions of an ill-perfused tumor vasculature. These results, along with our optical imaging data, suggest that significant portions of MNPs are retained in the tumor after MF removal and that MNPs in combination with drugs can be clinically effective in reducing tumor size. This strategy could be effectively used for imaging and treatment of superficial tumors such as cancer in the breast or various sarcomas. Further, hyperthemia induced using an alternating MF to the tumor tissue can potentially enhance the efficacy of anticancer drug loaded in MNPs.[32]

Optical methods are most suitable for preclinical studies to map changes in tumor vasculature or expression of receptors during tumor growth or in response to treatment.[33] MNPs with dual MRI and optical imaging characteristics could be particularly useful in detection of tumors *via* these two modalities to delineate the tumor periphery during surgical resection.[16,17] The next generation of nanoparticle-based research is directed at the consolidation of different functions into strategically engineered multifunctional nanoparticles to perform complementary roles in cancer therapy. Our MNPs have the potential to be developed as such a multifunctional theranostic agent.

CONCLUSIONS

We successfully developed MNPs with optical imaging properties and determined their dynamics of biodistribution *in vivo*, their localization and retention in tumor tissue when exposed to an externally applied MF, and their eventual clearance. With the use of highly sensitive optical imaging, it may be possible to evaluate how formulation characteristics (such as the interplay of physical characteristics and targeting ligands) may increase the accumulation of MNPs in tumors and eventually enhance drug delivery. MNPs with combined drug delivery and imaging properties can potentially be developed as an effective theranostic agent.

MATERIALS AND METHODS

Reagents. Pluronic F127 was a gift from BASF Corporation (Mt. Olive, NJ). Nitrogen-purged deionized water was used in all steps for MNP synthesis. Hydrophobic NIR dyes (SDB5700, SDA5177, SDA2826, SDA6825, and SDB5491) were purchased from H.W. Sands Corporation (Jupiter, FL). The following reagents were purchased from Fisher Scientific (Pittsburgh, PA): ammonium hydroxide (5 M), hydrochloric acid, iron(III) chloride hexahydrate ($FeCl_3 \cdot 6H_2O$, pure granulated, 99%), iron(II) chloride tetrahydrate ($FeCl_2 \cdot 4H_2O$, 99+%), and oleic acid (OA).

Magnetic Nanoparticle Synthesis and Characterization. Magnetite particles were synthesized by a co-precipitation reaction with Fe(II) and Fe(III) in the presence of ammonium hydroxide.[13] A 15 mL solution of 0.1 M Fe(II) was combined with 30 mL of 0.1 M Fe(III) and stirred for 20 min under a fume hood. Ammonium hydroxide (3 mL, 5 M) was added dropwise to the solution to precipitate magnetite particles. OA (100 mg) was added to the magnetite particles, and the solution was heated to 80 °C for 30 min to evaporate off ammonia gas. The solution was cooled to room temperature, washed once by magnetic separation, and resuspended in 45 mL of water. Pluronic F127 (100 mg) was added to the magnetite particle solution, and the mixture was covered and stirred overnight. The MNPs formed were washed three times with water by magnetic separation and resuspended in 10 mL of water after the final wash. The MNPs were centrifuged at 1000 rpm for 10 min at 4 °C to remove large aggregates, and the supernatant was collected and stored at 4 °C.

A 10 μL sample of MNPs was suspended in 4 mL of water, and the hydrodynamic size and zeta potential were determined by dynamic laser light scattering with the NICOMP 380 ZLS (Particle Sizing Systems, Santa Barbara, CA). A 1 mL sample of MNPs was lyophilized for 24 h and weighed to determine the MNP yield.

NIR Dye Loading in MNPs. MNPs (30 mg in 7 mL of water) were combined with 600 μL of 0.25−5.0% w/w NIR dye in ethanol with magnetic stirring. The solution was stirred overnight to allow the dyes to partition into the OA layer of the MNPs. The dye−MNPs were then washed three times by magnetic separation, and the washings were saved for analysis. The washings were centrifuged at 13 000 rpm to remove MNPs, and the supernatant was collected. A sample of the supernatant was diluted in ethanol, and the dye's peak absorbance was measured on a UV/vis spectrophotometer (DU 640B; Beckman Coulter, Brea, CA). Stock solutions (1 mg/mL) of each dye were prepared in ethanol, and dilutions were made in ethanol (0−10 μg/mL). Dye loading in MNPs was determined by subtracting the concentration of dye in the supernatant from the total amount of dye added.

Fluorescence Intensity and Photobleaching. The fluorescence intensity of the NIR dyes was measured by dropping 3 μL of dye (2.5−50.0 μg/mL in ethanol) onto filter paper and imaging with the Maestro EX NIR filter sets; the intensity (scaled counts/s) was determined from a circular ROI for each sample. The peak emission for each NIR dye was measured on the Maestro EX (Cambridge Research and Instrumentation, Woburn, MA). To determine if the iron-oxide quenched the fluorescence of dyes *in vivo*, mice were anesthetized with isoflurane and subcutaneously injected with 20 μL of dye−MNPs (1.0 mg MNP/mL; 2.5−50 μg dye/mL). ROIs surrounding the injection site were used to calculate the signal intensity (scaled counts/s).

Dye Toxicity. MCF7 breast cancer cells were treated with 2.0% w/w dye−MNPs at various concentrations to determine dye toxicity. MCF7 cells (100 μL) were seeded in 96-well plates (3000 cells/well) in DMEM (supplemented with 10% FBS and 1% penicillin streptomycin) and allowed to attach for 1 day. Medium was removed, and cells were treated with 2.0% w/w dye−MNPs (5−10 000 ng/mL dye, 0.25−50 μg/mL MNPs). The dye−MNPs were removed after 1 day, and cells were given fresh supplemented media. The medium was changed every 2 days thereafter, and the cells were not given any additional treatment. Five days after treatment, the medium was changed, and cell viability was determined using an MTS assay (CellTiter 96 Aqueous, Promega, Madison, WI). A growth curve was mathematically fit to the data to determine which dye concentration resulted in 50% inhibition of cell growth (IC_{50}).

Tumor Induction. The Cleveland Clinic Institutional Animal Care and Use Committee approved all animal procedures. Female athymic nude mice (20−30 g, nu/nu, Charles River, Wilmington, MA) were anesthetized by an intraperitoneal injection of 100−150 mg/kg body weight of ketamine and 10 mg/kg xylazine. A 100 μL suspension of MCF7 cells grown on microparticle scaffolds prepared in our laboratory using a previously established protocol was used for tumor innocation.[34] Cells were grown on the scaffold for 6 days. The scaffold, with 500 000 cells, was suspended in 100 μL of D-PBS and combined with 100 μL of Matrigel (BD Biosciences, Bedford, MA) and injected in the uppermost left mammary complex of each mouse. This 3-D structure for tumor induction forms tumors of consistent size more frequently than cells injected in Matrigel alone. A 17-β-estradiol pellet (1.5 mg, 90 day release; Innovative Research of America, Sarasota, FL) was implanted subcutaneously in the right flank of each mouse to promote tumor growth. Tumor growth was regularly measured with calipers, and tumor volume was calculated as (length × width^2)/2. Mice were treated when tumors reached ~300 mm^3. Mice were kept on the Teklad Global 18% protein rodent diet (2018S), an alfalfa-free, wheat-based diet (Harlan Laboratories, Indianapolis, IN), to reduce autofluorescence.

Biodistribution of NIR Dye−MNPs. The distribution of dye−MNPs in a mouse with an MCF7 xenograft breast tumor was determined with the Maestro EX. A mouse anesthetized with isoflurane was injected intravenously with 100 μL of 5491 dye−MNPs (4.9 mg MNPs/mL, 0.25 mg dye/mL) and imaged daily until the dye−MNPs were no longer detected. The Maestro Blue filter set was used to image the mouse autofluorescence, and the NIR filter was used to detect the 5491 dye−MNPs.

Influence of a Magnetic Field on the Localization of NIR Dye−MNPs in Tumor-Bearing Mice. The effect of an externally applied MF on the localization of NIR dye−MNPs in an MCF7 xenograft breast tumor was determined by placing a magnet (Neodymium Iron Boron, 1.25 × 1.25 × 0.3 cm, Gauss: 12200, Edmund Scientific, Tonawanda, NY) over the surface of a tumor with Steri-Strip tape (3M Health Care, St. Paul, MN) while mice were anesthetized with isoflurane. Control mice, also anesthetized with isoflurane, did not have a magnet placed over the tumor. While anesthetized, mice were injected with 100 μL of 0.25% w/w 6825 dye−MNPs in mannitol citrate buffer (86.8 mg/kg MNPs, 0.22 mg/kg dye). After 1 h, the magnet was removed from the mice. Mice were imaged with the Maestro EX NIR filter set 24 h post-injection, injected with a lethal dose of sodium pentobarbital, and perfused *via* intracardiac injection of saline to remove circulating MNPs. The tumors were collected and immediately imaged with the Maestro EX NIR filter set. Tumors were weighed and homogenized in sterile Milli-Q water at 0.1 g/mL. The homogenate was serially diluted to a final volume of 100 μL in each well in a white 96-well plate, and the fluorescence was measured with the Maestro EX NIR filter set. Dye−MNPs (0.25% w/w 6825 dye−MNPs, 0−100 ng dye) were suspended in tumor homogenates of an untreated animal for a standard plot. The average of the diluted samples in the linear region of the standard plot was compared with the unknown samples to determine the amount of dye present in each tumor. Data were normalized based on the position of each well under fluorescent light.

Statistical Analysis. Statistical analyses were performed using Student's *t* test. The differences were considered significant for *p* values of ≤0.05.

Acknowledgment. The study is funded by Grant R01 EB005822 (to V.L.) from the National Institute of Biomedical Imaging and Bioengineering of the National Institutes of Health. S.P.F. is a predoctoral student in Cleveland Clinic's Molecular Medicine Ph.D. Program, which is funded by the "Med into Grad" initiative of the Howard Hughes Medical Institute (http://www.lerner.ccf.org/molcmed/phd/).

REFERENCES AND NOTES

1. Medarova, Z.; Rashkovetsky, L.; Pantazopoulos, P.; Moore, A. Multiparametric Monitoring of Tumor Response to Chemotherapy by Noninvasive Imaging. *Cancer Res.* **2009**, *69*, 1182–1189.
2. Weissleder, R.; Pittet, M. J. Imaging in the Era of Molecular Oncology. *Nature* **2008**, *452*, 580–589.
3. Baker, M. Whole-Animal Imaging: The Whole Picture. *Nature* **2010**, *463*, 977–980.
4. Wan, J.; Meng, X.; Liu, E.; Chen, K. Incorporation of Magnetite Nanoparticle Clusters in Fluorescent Silica Nanoparticles for High-Performance Brain Tumor Delineation. *Nanotechnology* **2010**, *21*, 235104.
5. Mandal, S. K.; Lequeux, N.; Rotenberg, B.; Tramier, M.; Fattaccioli, J.; Bibette, J.; Dubertret, B. Encapsulation of Magnetic and Fluorescent Nanoparticles in Emulsion Droplets. *Langmuir* **2005**, *21*, 4175–4179.
6. Lim, Y. T.; Noh, Y. W.; Han, J. H.; Cai, Q. Y.; Yoon, K. H.; Chung, B. H. Biocompatible Polymer-Nanoparticle-Based Bimodal Imaging Contrast Agents for the Labeling and Tracking of Dendritic Cells. *Small* **2008**, *4*, 1640–1645.
7. Sun, C.; Du, K.; Fang, C.; Bhattarai, N.; Veiseh, O.; Kievit, F.; Stephen, Z.; Lee, D.; Ellenbogen, R. G.; Ratner, B.; *et al.* PEG-Mediated Synthesis of Highly Dispersive Multifunctional Superparamagnetic Nanoparticles: Their Physicochemical Properties and Function *In Vivo*. *ACS Nano* **2010**, *4*, 2402–2410.
8. Wang, L.; Neoh, K. G.; Kang, E. T.; Shuter, B.; Wang, S. C. Biodegradable Magnetic-Fluorescent Magnetite/Poly(DL-Lactic acid-*co*-α,β-Malic acid) Composite Nanoparticles for Stem Cell Labeling. *Biomaterials* **2010**, *31*, 3502–3511.
9. Jarzyna, P. A.; Skajaa, T.; Gianella, A.; Cormode, D. P.; Samber, D. D.; Dickson, S. D.; Chen, W.; Griffioen, A. W.; Fayad, Z. A.; Mulder, W. J. Iron Oxide Core Oil-in-Water Emulsions as a Multifunctional Nanoparticle Platform for Tumor Targeting and Imaging. *Biomaterials* **2009**, *30*, 6947–6954.
10. Kumar, R.; Roy, I.; Ohulchanskky, T. Y.; Vathy, L. A.; Bergey, E. J.; Sajjad, M.; Prasad, P. N. *In Vivo* Biodistribution and Clearance Studies Using Multimodal Organically Modified Silica Nanoparticles. *ACS Nano* **2010**, *4*, 699–708.
11. Moore, A.; Medarova, Z.; Potthast, A.; Dai, G. *In Vivo* Targeting of Underglycosylated Muc-1 Tumor Antigen Using a Multimodal Imaging Probe. *Cancer Res.* **2004**, *64*, 1821–1827.
12. Uzgiris, E. E.; Sood, A.; Bove, K.; Grimmond, B.; Lee, D.; Lomnes, S. A Multimodal Contrast Agent for Preoperative MR Imaging and Intraoperative Tumor Margin Delineation. *Technol. Cancer Res. Treat.* **2006**, *5*, 301–309.
13. Jain, T. K.; Morales, M. A.; Sahoo, S. K.; Leslie-Pelecky, D. L.; Labhasetwar, V. Iron Oxide Nanoparticles for Sustained Delivery of Anticancer Agents. *Mol. Pharmaceutics* **2005**, *2*, 194–205.
14. Jain, T. K.; Richey, J.; Strand, M.; Leslie-Pelecky, D. L.; Flask, C. A.; Labhasetwar, V. Magnetic Nanoparticles with Dual Functional Properties: Drug Delivery and Magnetic Resonance Imaging. *Biomaterials* **2008**, *29*, 4012–4021.
15. Jain, T. K.; Foy, S. P.; Erokwu, B.; Dimitrijevic, S.; Flask, C. A.; Labhasetwar, V. Magnetic Resonance Imaging of Multifunctional Pluronic Stabilized Iron-Oxide Nanoparticles in Tumor-Bearing Mice. *Biomaterials* **2009**, *30*, 6748–6756.
16. Kircher, M. F.; Mahmood, U.; King, R. S.; Weissleder, R.; Josephson, L. A Multimodal Nanoparticle for Preoperative Magnetic Resonance Imaging and Intraoperative Optical Brain Tumor Delineation. *Cancer Res.* **2003**, *63*, 8122–8125.
17. Kajimoto, Y.; Kuroiwa, T.; Miyatake, S.; Ichioka, T.; Miyashita, M.; Tanaka, H.; Tsuji, M. Use of 5-Aminolevulinic Acid in Fluorescence-Guided Resection of Meningioma with High Risk of Recurrence. Case Report. *J. Neurosurg.* **2007**, *106*, 1070–1074.
18. Lubbe, A. S.; Bergemann, C.; Huhnt, W.; Fricke, T.; Riess, H.; Brock, J. W.; Huhn, D. Preclinical Experiences with Magnetic Drug Targeting: Tolerance and Efficacy. *Cancer Res.* **1996**, *56*, 4694–4701.
19. Brooksby, B.; Pogue, B. W.; Jiang, S.; Dehghani, H.; Srinivasan, S.; Kogel, C.; Tosteson, T. D.; Weaver, J.; Poplack, S. P.; Paulsen, K. D. Imaging Breast Adipose and Fibroglandular Tissue Molecular Signatures by Using

Hybrid MRI-Guided Near-Infrared Spectral Tomography. *Proc. Natl. Acad. Sci. U.S.A.* **2006**, *103*, 8828–8833.
20. Jain, T. K.; Reddy, M. K.; Morales, M. A.; Leslie-Pelecky, D. L.; Labhasetwar, V. Biodistribution, Clearance, and Biocompatibility of Iron Oxide Magnetic Nanoparticles in Rats. *Mol. Pharmaceutics* **2008**, *5*, 316–327.
21. Maeda, H.; Wu, J.; Sawa, T.; Matsumura, Y.; Hori, K. Tumor Vascular Permeability and the EPR Effect in Macromolecular Therapeutics: A Review. *J. Controlled Release* **2000**, *65*, 271–284.
22. Owens, D. E., III; Peppas, N. A. Opsonization, Biodistribution, and Pharmacokinetics of Polymeric Nanoparticles. *Int. J. Pharm.* **2006**, *307*, 93–102.
23. Stolnik, S.; Illum, L.; Davis, S. S. Long Circulating Microparticulate Drug Carriers. *Adv. Drug Delivery Rev.* **1995**, *16*, 195–214.
24. Yuan, F.; Dellian, M.; Fukumura, D.; Leunig, M.; Berk, D. A.; Torchilin, V. P.; Jain, R. K. Vascular Permeability in a Human Tumor Xenograft: Molecular Size Dependence and Cutoff Size. *Cancer Res.* **1995**, *55*, 3752–3756.
25. Yang, Z.; Leon, J.; Martin, M.; Harder, J. W.; Zhang, R.; Liang, D.; Lu, W.; Tian, M.; Gelovani, J. G.; Qiao, A.; *et al.* Pharmacokinetics and Biodistribution of Near-Infrared Fluorescence Polymeric Nanoparticles. *Nanotechnology.* **2009**, *20*, 165101.
26. Taupitz, M.; Wagner, S.; Schnorr, J.; Kravec, I.; Pilgrimm, H.; Bergmann-Fritsch, H.; Hamm, B. Phase I Clinical Evaluation of Citrate-Coated Monocrystalline Very Small Superparamagnetic Iron Oxide Particles as a New Contrast Medium for Magnetic Resonance Imaging. *Invest. Radiol.* **2004**, *39*, 394–405.
27. McCarthy, J. R.; Weissleder, R. Multifunctional Magnetic Nanoparticles for Targeted Imaging and Therapy. *Adv. Drug Delivery Rev.* **2008**, *60*, 1241–1251.
28. Yang, Y.; Jiang, J. S.; Du, B.; Gan, Z. F.; Qian, M.; Zhang, P. Preparation and Properties of a Novel Drug Delivery System with Both Magnetic and Biomolecular Targeting. *J. Mater. Sci. Mater. Med.* **2009**, *20*, 301–307.
29. Martina, M. S.; Fortin, J. P.; Fournier, L.; Menager, C.; Gazeau, F.; Clement, O.; Lesieur, S. Magnetic Targeting of Rhodamine-Labeled Superparamagnetic Liposomes to Solid Tumors: *In Vivo* Tracking by Fibered Confocal Fluorescence Microscopy. *Mol. Imaging* **2007**, *6*, 140–146.
30. Luciani, A.; Wilhelm, C.; Bruneval, P.; Cunin, P.; Autret, G.; Rahmouni, A.; Clement, O.; Gazeau, F. Magnetic Targeting of Iron-Oxide-Labeled Fluorescent Hepatoma Cells to the Liver. *Eur Radiol.* **2009**, *19*, 1087–1096.
31. Lubbe, A. S.; Bergemann, C.; Riess, H.; Schriever, F.; Reichardt, P.; Possinger, K.; Matthias, M.; Dorken, B.; Herrmann, F.; Gurtler, R.; *et al.* Clinical Experiences with Magnetic Drug Targeting: A Phase I Study with 4′-Epidoxorubicin in 14 Patients with Advanced Solid Tumors. *Cancer Res.* **1996**, *56*, 4686–4693.
32. Needham, D.; Anyarambhatla, G.; Kong, G.; Dewhirst, M. W. A New Temperature-Sensitive Liposome for Use with Mild Hyperthermia: Characterization and Testing in a Human Tumor Xenograft Model. *Cancer Res.* **2000**, *60*, 1197–1201.
33. Hilger, I.; Leistner, Y.; Berndt, A.; Fritsche, C.; Haas, K. M.; Kosmehl, H.; Kaiser, W. A. Near-Infrared Fluorescence Imaging of Her-2 Protein Over-Expression in Tumour Cells. *Eur. Radiol.* **2004**, *14*, 1124–1129.
34. Horning, J. L.; Sahoo, S. K.; Vijayaraghavalu, S.; Dimitrijevic, S.; Vasir, J. K.; Jain, T. K.; Panda, A. K.; Labhasetwar, V. 3-D Tumor Model for *In Vitro* Evaluation of Anticancer Drugs. *Mol. Pharmaceutics* **2008**, *5*, 849–862.